Cooperation Mechanism Design for Integrated Electricity-Heat Systems with Information Asymmetry

Jizhong Zhu, *Fellow*, *IEEE*, Haohao Zhu, Weiye Zheng, Shenglin Li, and Junwei Fan

***Abstract*—Cooperation between electric power networks (EPNs) and district heating networks (DHNs) has been extensively studied under the assumption that all information exchanged is authentic. However, EPNs and DHNs belonging to different entities may result in marketing fraud. This paper proposes a cooperation mechanism for integrated electricity-heat systems (IEHSs) to overcome information asymmetry. First, a fraud detection method based on multiparametric programming with guaranteed feasibility reveals the authenticity of the information. Next, all honest entities are selected to form a coalition. Furthermore, to maintain operational independence and distribute benefits fairly, Benders decomposition is enhanced to calculate Shapley values in a distributed fashion. Finally, the cooperative surplus generated by the coalition is allocated according to the marginal contribution of each entity. Numerical results show that the proposed mechanism stimulates cooperation while achieving Pareto optimality under asymmetric information.**

***Index Terms*—Information asymmetry, integrated electricity-heat system, Benders decomposition, fraud detection, Shapley value.**

I. Introduction

DISTRICT heating networks (DHNs) give electric power networks (EPNs) a window to accommodate more renewable energy. However, heat-driven policy throws the flexibility of combined heat and power (CHP) units into question [1]. For instance, in northeastern China, the generation of CHP units depends on heat loads. It results in more than 1500 GWh of wind power being curtailed in 2013 [2]. Studies on integrated electricity-heat systems (IEHSs) aim to address this challenge. The installation of heat storage tanks [3], heat pumps [4], or electric boilers [5] promises to increase the flexibility of EPNs while increasing the investment cost. A more appealing prospect is to use the pipeline heat storage of DHNs [6].

Manuscript received: May 24, 2022; revised: September 2, 2022; accepted: October 17, 2022. Date of CrossCheck: October 17, 2022. Date of online publication: November 9, 2022.

This work was supported by National Natural Science Foundation of China (No. 52177087).

J. Zhu (corresponding author), H. Zhu, W. Zheng, S. Li, and J. Fan are with the School of Electric Power Engineering, South China University of Technology, Guangzhou 510641, China (e-mail: zhujz@scut.edu.cn; epzhh@mail.scut.edu.cn; wzheng@scut.edu.cn; iamlshl@126.com; epxiaowait@mail.scut.edu.cn).

DOI: 10.35833/MPCE.2022.000301

The centralized scheduling of IEHSs [7], [8] is divorced from the reality that EPNs and DHNs are separate entities. It is impractical for EPNs and DHNs to share private information including topological structures, model parameters, and operating status. Fortunately, decentralized scheduling facilitates operation independence and privacy protection. EPNs and DHNs only exchange boundary information such as Lagrange multipliers in dual decomposition [9]-[12] or feasibility cuts and optimality cuts generated in Benders decomposition [13]-[15]. Optimality condition decomposition for IEHS dispatch is employed in [16]. Distributed economic dispatch of IEHSs is introduced in [17]. Such studies, however, ignore incentive compatibility among multiple entities.

IEHS dispatch based on holistic optimization may lead to incentive incompatibility. Tapping into pipeline heat storage can improve the operation flexibility of EPNs, but it will incur higher heat losses and more operating cost for DHNs. Therefore, DHNs based on individual rationality has little incentive to cooperate with EPNs. Reference [18] proposes a hybrid energy sharing framework involving multiple microgrids in IEHSs. Generalized locational marginal pricing in an integrated electricity and heat market is discussed in [19]. Reference [20] proposes a distributed dispatch solution for IEHSs under variable flow, where the model is bi-level, mixed-integer, and nonlinear. Reference [21] examines IEHSs from a market perspective. Reference [22] proposes an electricity, heating, and cooling trading model for the interaction between the multi-energy service provider and multi-energy consumer by using bi-level programming. A cost-sharing mechanism based on transfer payments is designed in [23], where EPNs share a part of payoffs of renewable energy accommodation with DHNs to promote cooperation. Nevertheless, these studies ignore the problem of information asymmetry among different entities. More specifically, almost all studies take for granted that the information exchanged between EPNs and DHNs is completely authentic.

Fairness is the basis of transactions between different stakeholders. However, EPNs and DHNs with information asymmetry can result in marketing fraud, which means that DHNs exaggerate the operating cost in IEHS dispatch. The structure of IEHS dispatch under asymmetric information is shown in Fig. 1. EPNs and DHNs are controlled by different operators. Both CHP units operated by EPNs and heating boilers (HBs) managed by DHNs can supply heat. DHN op-

erators send the operating cost of DHN C_{H} to EPN operators. To encourage cooperation, EPN operators share a portion of the payoffs of renewable energy accommodation W_{E} with DHN operators.

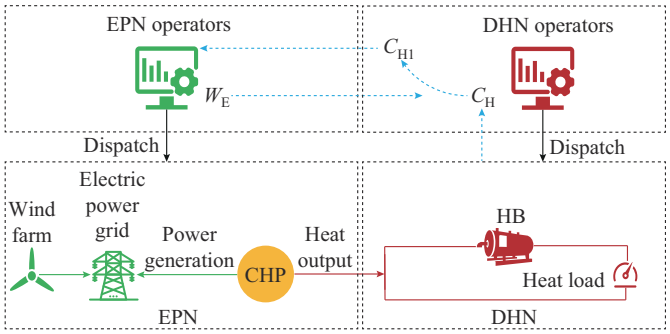

Fig. 1. Structure of IEHS dispatch under asymmetric information.

However, EPN operators do not know whether C_{H} is authentic or not due to operational independence. It is conceivable that some DHN operators will increase C_{H} to obtain more compensation from EPN operators. For example, some DHN operators send the increased operating cost of HBs C_{H1} to EPN operators. Since C_{H1} is larger than C_{H}, EPN operators will compensate DHN operators more accordingly. The problem boils down to marketing fraud caused by information asymmetry. If DHN operators exaggerate losses to get more compensation, and even cause damage to the interests of EPN operators, it will be difficult for both parties to cooperate, so it is necessary to guarantee the fairness of the transaction. An intuitive solution is to design a fraud detection method to overcome information asymmetry.

The proposed fraud detection method can disclose the authenticity of information exchanged between EPNs and DHNs. All honest entities are selected to form a coalition. Honest entities are dispatched coordinately; dishonest entities are dispatched separately. The only challenge that remains now is how to fairly and efficiently allocate the cooperative surplus generated by the coalition. EPNs give transfer payments to DHNs, but it is laborious to calculate the optimal sharing ratio [23]. Combined scheduling of IEHSs considering mutual benefit is discussed in [24]. However, the problem of feasibility has not been fully handled. In addition, it cannot cover the cases with multiple EPNs and DHNs. In a sense, IEHS dispatch is a cooperative game. The Shapley value provides a practical solution for benefit distribution among several players in a coalition [25]. These research works, however, cannot overcome information asymmetry and distribute benefits fairly in a decentralized manner involving multiple entities.

Although IEHS dispatch has been investigated in numerous previous literature, it cannot bridge the gap between optimal utilization of energy resources and information asymmetry between EPNs and DHNs. Cooperation between EPNs and DHNs has been extensively studied under the assumption that all information exchanged is authentic. Besides, EPNs and DHNs belonging to different entities may lead to marketing fraud. Furthermore, how to encourage cooperation while achieving Pareto optimality under asymmetric information remains an open challenge. In conclusion, IEHS dispatch should fully guarantee fraud detection, privacy protection, and incentive compatibility under asymmetric information. Thus, we propose a cooperation mechanism for IEHSs with information asymmetry. Highlights of our original contributions are as follows:

1) A fraud detection method based on multiparameter programming with guaranteed feasibility is proposed to overcome information asymmetry. Specifically, it reveals the authenticity of information exchanged among multiple entities.

2) All honest entities are selected to form a coalition and coordinate scheduling based on the proposed fraud detection method. In contrast, dishonest entities submitting false information are dispatched separately.

3) To preserve privacy and achieve incentive compatibility, the enhanced Benders decomposition is proposed to calculate Shapley values in a distributed manner.

4) The proposed mechanism stimulates DHNs to cooperate with EPNs while achieving Pareto optimality under asymmetric information.

The remainder of the paper is structured as follows. We present an IEHS dispatch model under asymmetric information in Section II. Next, we further discuss the problem of information asymmetry when EPNs cooperate with DHNs. A distributed algorithm with fraud detection is employed in Section III. In Section VI, we establish a fair benefit distribution mechanism for the coalition by calculating Shapley values. The case study justifies the effectiveness of the proposed cooperation mechanism in Section V. Finally, conclusions are given in Section VI.

II. IEHS Dispatch Model Under Asymmetric Information

This section describes an IEHS dispatch model under asymmetric information in a compact form. In addition, we explore the causes of information asymmetry and its repercussions.

A. IEHS Dispatch Model

The IEHS dispatch model is presented in a compact form.

$$\min_{\{\boldsymbol{x}_{\mathrm{E}},\boldsymbol{h}_{\mathrm{C}}\},\{\boldsymbol{h}_{\mathrm{H}(a)},\boldsymbol{x}_{\mathrm{H}(a)}\}} \left\{C_{\mathrm{E}}\left(\boldsymbol{x}_{\mathrm{E}},\boldsymbol{h}_{\mathrm{C}}\right)+\sum_{a=1}^{n}C_{\mathrm{H}(a)}\left(\boldsymbol{h}_{\mathrm{H}(a)}\right)\right\} \tag{1}$$

s.t.

$$\boldsymbol{D}_{\mathrm{E}}\boldsymbol{x}_{\mathrm{E}}+\boldsymbol{B}_{\mathrm{C}}\boldsymbol{h}_{\mathrm{C}}\le\boldsymbol{b}_{\mathrm{E}} \tag{2}$$

$$\boldsymbol{F}_{\mathrm{C}(a)}\boldsymbol{h}_{\mathrm{C}}+\boldsymbol{F}_{\mathrm{H}(a)}\boldsymbol{h}_{\mathrm{H}(a)}+\boldsymbol{D}_{\mathrm{H}(a)}\boldsymbol{x}_{\mathrm{H}(a)}=\boldsymbol{f}_{\mathrm{H}(a)} \tag{3}$$

$$\underline{\boldsymbol{x}}_{\mathrm{H}(a)}\le\boldsymbol{x}_{\mathrm{H}(a)}\le\bar{\boldsymbol{x}}_{\mathrm{H}(a)} \tag{4}$$

$$\underline{\boldsymbol{h}}_{\mathrm{H}(a)}\le\boldsymbol{h}_{\mathrm{H}(a)}\le\bar{\boldsymbol{h}}_{\mathrm{H}(a)} \tag{5}$$

$$a=1,2,\ldots,n \tag{6}$$

where $\boldsymbol{x}_{\mathrm{E}}=\left[\boldsymbol{p}_{\mathrm{g}},\boldsymbol{ru}_{\mathrm{g}},\boldsymbol{rd}_{\mathrm{g}},\boldsymbol{\theta}_{\mathrm{t}},\boldsymbol{p}_{\mathrm{g}}^{\mathrm{w}},\boldsymbol{\alpha}_{\mathrm{g}}\right]^{\mathrm{T}}$ is the vector of internal variables of EPNs, $\boldsymbol{p}_{\mathrm{g}}$ is the electric power generation, $\boldsymbol{ru}_{\mathrm{g}}$ and $\boldsymbol{rd}_{\mathrm{g}}$ are the upward and downward spinning reserve demands of CHP units and thermal generating units, respectively, $\boldsymbol{\theta}_{\mathrm{t}}$ is the phase angle of buses, $\boldsymbol{p}_{\mathrm{g}}^{\mathrm{w}}$ is the electric power generation of wind farms, $\boldsymbol{\alpha}_{\mathrm{g}}$ is the extreme point coefficient

of CHP units; $C_{\mathrm{E}}(\cdot)$ is the cost of EPNs; $C_{\mathrm{H}(a)}(\cdot)$ is the cost of the a^{th} DHN; $\boldsymbol{x}_{\mathrm{H}(a)}$ is the vector of internal variables of the a^{th} DHN; $\boldsymbol{h}_{\mathrm{C}}$ is the heat output supplied by CHP units; $\underline{\boldsymbol{x}}_{\mathrm{H}(a)}$ and $\bar{\boldsymbol{x}}_{\mathrm{H}(a)}$ are the lower and upper limits of the vector of internal variables of the a^{th} DHN, respectively; $\boldsymbol{h}_{\mathrm{H}(a)}$ is the heat generation supplied by HBs in the a^{th} DHN; $\underline{\boldsymbol{h}}_{\mathrm{H}(a)}$ and $\bar{\boldsymbol{h}}_{\mathrm{H}(a)}$ are the lower and upper limits of heat generation supplied by HBs in the a^{th} DHN, respectively; n is the number of DHN; and $\boldsymbol{D}_{\mathrm{E}}$, $\boldsymbol{B}_{\mathrm{C}}$, $\boldsymbol{b}_{\mathrm{E}}$, $\boldsymbol{F}_{\mathrm{C}(a)}$, $\boldsymbol{F}_{\mathrm{H}(a)}$, $\boldsymbol{D}_{\mathrm{H}(a)}$, and $\boldsymbol{f}_{\mathrm{H}(a)}$ are all coefficient matrixes or vectors.

Constraint (2) includes active power balance (A33), spinning reserve requirements (A34)-(A38), ramping limits (A39), and power network constraints (A40) and (A41). Constraint (3) refers to constraints of the a^{th} DHN, including (A1), (A4)-(A18). Constraint (4) refers to the operating bounds of the a^{th} DHN, as shown in (A3), (A19), and (A20). Please refer to the Appendix A for detailed definitions and descriptions of the model.

B. Discussion on Problem of Information Asymmetry

We further discuss the problem of information asymmetry between EPNs and DHNs. First, the differences between combined dispatch and separate dispatch are compared. Next, we evaluate the operating cost of EPNs, DHNs, and IEHSs in two dispatch models. Finally, the causes and repercussions of information asymmetry are investigated.

In separated dispatch, DHNs attempt to keep heating supply temperature at CHP unit node constant all time and submit the heat loads to EPNs [15]. Next, the economic dispatch problem is solved by including additional heat supply constraints. In this case, heat loads are determined by (A3), (A15), (A16), and (7).

$$\tau_{g,t}^{\mathrm{GS}} = \Gamma_{g,0}^{\mathrm{GS}} \quad \forall g \in \mathcal{G}^{\mathrm{CHP}}, t \in \mathcal{T} \tag{7}$$

where $\tau_{g,t}^{\mathrm{GS}}$ is the supply temperature of CHP unit g; $\Gamma_{g,0}^{\mathrm{GS}}$ is the initial supply temperature of CHP unit g; $\mathcal{G}^{\mathrm{CHP}}$ is the set of CHP units; and $\mathcal{T}$ is the set of dispatch horizons.

Since the ambient temperature is higher during the day and lower at night, heat loads are lower during the day and higher at night. Nonetheless, heat loads and electricity loads are inverse. The peak-to-valley distribution between forecasted wind power output and electricity loads is also opposite. In the heat-driven model, the electricity output of CHP units depends on heat loads. Since heat loads are high at night, CHP units generate a lot of electricity while producing heat, and the wind power output must be reduced.

In combined dispatch, the DHN is heated early in the heat load trough. At night, CHP units will be operated at a low output level to free up space for wind power accommodation. Simultaneously, relatively more expensive HBs will replace CHP units for heat supply. The DHN makes full use of pipeline energy storage in combined dispatch and provides the EPN with greater flexibility, but at the expense of higher operating cost and heat losses for the DHN.

As shown in Table I, C'_{E}, C'_{H}, and C'_{IEHS} are the costs of the EPN, DHN, and IEHS in separated dispatch, respectively; C_{IEHS} is the cost of the IEHS in combined dispatch. To be specific, C_{E} and C'_{E} include operating cost of thermal generating units, operating cost of CHP units, and wind curtailment penalty in separated dispatch and combined dispatch, respectively. C_{H} and C'_{H} include the operating cost of HBs in separated dispatch and combined dispatch, respectively. The sum of $C_{\mathrm{E}}/C'_{\mathrm{E}}$ and the sum of $C_{\mathrm{H}}/C'_{\mathrm{H}}$ are the total costs of the IEHS in separated dispatch and combined dispatch, respectively.

TABLE I
COSTS OF EPN, DHN, AND IEHS UNDER DIFFERENT DISPATCH METHODS

Method	Cost of EPN ($)	Cost of DHN ($)	Cost of IEHS ($)
Separated dispatch	C'_{E}	C'_{H}	C'_{IEHS}
Combined dispatch	$C_{\mathrm{E}}\downarrow$	$C_{\mathrm{H}}\uparrow$	$C_{\mathrm{IEHS}}\downarrow$
With compensation	$(C_{\mathrm{E}}+W_{\mathrm{E}})\downarrow$	$(C_{\mathrm{E}}-W_{\mathrm{E}})\downarrow$	$C_{\mathrm{IEHS}}\downarrow$

According to the previous analysis, we conclude that C_{E} is smaller than C'_{E}, C_{H} is greater than C'_{H}, and C_{IEHS} is smaller than C'_{IEHS}. As a consequence, the cost of DHN increases, and the cost of EPN decreases. To stimulate cooperation, the EPN shares a part of the benefits of renewable energy accommodation W_{E} with the DHN. Therefore, the costs of both EPN and DHN decrease. In other words, all entities in combined dispatch achieve incentive compatibility.

The above analysis assumes that all information exchanged between EPNs and DHNs is authentic. However, due to information asymmetry, EPN operators do not know whether C_{H} is real or fake. In order to obtain further compensation, some DHN operators increase C_{H}. Information asymmetry results in marketing fraud. Designing a fraud detection method to constrain individual behavior is an obvious solution to overcoming information asymmetry.

III. DISTRIBUTED ALGORITHM WITH FRAUD DETECTION

A distributed algorithm with fraud detection is proposed in this section. Specific procedures based on multiparametric programming with guaranteed feasibility disclose the authenticity of the information exchanged among different entities. Next, all honest entities are selected to form a coalition. Entities in the coalition are dispatched in coordination, whereas dishonest entities are dispatched separately.

Distributed scheduling facilitates operational independence and protects private information. In this section, IEHS dispatch problem is decomposed into EPN master problem and DHN subproblems through Benders decomposition. In particular, to ensure all subproblems are always feasible, each DHN sends a predefined feasibility cut to EPN before iteration. We introduce a corollary about multiparameter programming and convex optimization first. Please refer to Appendix A for detailed definitions and descriptions of the model.

Corollary: because IEHS dispatch is a convex optimization problem, the local optimal solution of this problem is also its global optimal solution. If the solution of the master problem lies within the boundary of the critical region *CR* instead of on it, it is both a local optimal solution and a global one. To be specific, the solution is supposed to lie on the boundary of the critical region before the master problem converges to the global optimal solution. The local optimal

costs *LOC* in the two adjacent critical regions are equal during each iteration [26].

Figure 2 shows the space of parameters $\boldsymbol{h}_{\mathrm{C}}$. *CR*1, *CR*2, and *CR*3 are all critical regions. They form the space of parameters $\boldsymbol{h}_{\mathrm{C}}$. Figure 3 shows that the local optimal costs of adjacent critical regions are equal. $LOC(\boldsymbol{h}_{\mathrm{C}})$ is the local optimal cost.

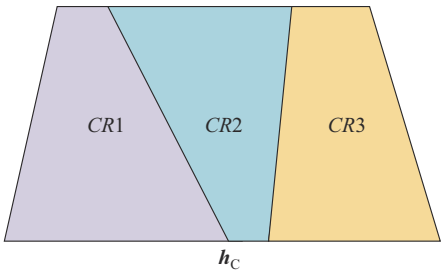

Fig. 2. Space of parameters $\boldsymbol{h}_{\mathrm{C}}$.

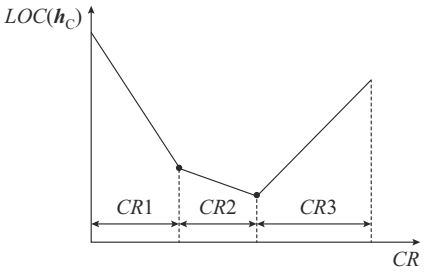

Fig. 3. Local optimal costs of adjacent critical regions.

The distributed algorithm with fraud detection includes the following details.

1) S1: initialize iteration number $k=1$ and optimal value $y^{(0)}=\infty$. In particular, each DHN sends a predefined feasibility cut to EPN.

2) S2: EPN optimizes the improved master problem (8) and expresses the optimal solution as $\boldsymbol{x}_{\mathrm{E}}^{(k)}$ and $\boldsymbol{h}_{\mathrm{C}}^{(k)}$. $\boldsymbol{x}_{\mathrm{E}}^{(k)}$ is the vector of internal variables of EPNs in the k^{th} iteration. $\boldsymbol{h}_{\mathrm{C}}^{(k)}$ is the heat output supplied by CHP units in the k^{th} iteration.

$$\begin{cases} \min\limits_{\boldsymbol{x}_{\mathrm{E}},\boldsymbol{h}_{\mathrm{C}},\boldsymbol{h}_{\mathrm{H}(a)}} C_{\mathrm{E}}(\boldsymbol{x}_{\mathrm{E}},\boldsymbol{h}_{\mathrm{C}}) \\ \text{s.t. } \boldsymbol{D}_{\mathrm{E}}\boldsymbol{x}_{\mathrm{E}}+\boldsymbol{B}_{\mathrm{C}}\boldsymbol{h}_{\mathrm{C}}\le\boldsymbol{b}_{\mathrm{E}} \\ \quad \boldsymbol{G}_{\mathrm{C}(a)}^{\mathrm{FC}}\boldsymbol{h}_{\mathrm{C}}+\boldsymbol{G}_{\mathrm{H}(a)}^{\mathrm{FC}}\boldsymbol{h}_{\mathrm{H}(a)}\le\boldsymbol{g}_{(a)}^{\mathrm{FC}} \quad a=1,2,\ldots,n \end{cases} \tag{8}$$

where $\boldsymbol{G}_{\mathrm{C}(a)}^{\mathrm{FC}}$, $\boldsymbol{G}_{\mathrm{H}(a)}^{\mathrm{FC}}$, and $\boldsymbol{g}_{(a)}^{\mathrm{FC}}$ are the coefficient matrixes or vectors, and the detailed descriptions are available in the Appendix A.

3) S3: EPN provides fixed boundary variable $\boldsymbol{h}'_{\mathrm{C}}$ for each DHN. $\boldsymbol{h}'_{\mathrm{C}}$ is a copy of $\boldsymbol{h}_{\mathrm{C}}^{(k)}$. Each DHN optimizes its subproblem. In the k^{th} iteration, the a^{th} DHN subproblem is described as:

$$\begin{cases} \eta_{\mathrm{H}(a)}\left(\boldsymbol{h}_{\mathrm{C}}^{(k)}\right)=\min\limits_{\boldsymbol{h}'_{\mathrm{C}},\boldsymbol{h}_{\mathrm{H}(a)},\boldsymbol{x}_{\mathrm{H}(a)}} C_{\mathrm{H}(a)}\left(\boldsymbol{h}_{\mathrm{H}(a)}\right) \\ \text{s.t. } \boldsymbol{h}'_{\mathrm{C}}=\boldsymbol{h}_{\mathrm{C}}^{(k)} \quad \boldsymbol{\beta}_{(a)}^{(k)} \\ \quad \boldsymbol{F}_{\mathrm{C}(a)}\boldsymbol{h}'_{\mathrm{C}}+\boldsymbol{F}_{\mathrm{H}(a)}\boldsymbol{h}_{\mathrm{H}(a)}+\boldsymbol{D}_{\mathrm{H}(a)}\boldsymbol{x}_{\mathrm{H}(a)}=\boldsymbol{f}_{\mathrm{H}(a)} \quad \boldsymbol{\lambda}_{(a)}^{(k)} \\ \quad \boldsymbol{G}_{\mathrm{C}(a)}^{\mathrm{FC}}\boldsymbol{h}'_{\mathrm{C}}+\boldsymbol{G}_{\mathrm{H}(a)}^{\mathrm{FC}}\boldsymbol{h}_{\mathrm{H}(a)}\le\boldsymbol{g}_{(a)}^{\mathrm{FC}} \quad \boldsymbol{\mu}_{(a)}^{(k)} \end{cases} \tag{9}$$

where $\boldsymbol{\beta}_{(a)}^{(k)}$, $\boldsymbol{\lambda}_{(a)}^{(k)}$, and $\boldsymbol{\mu}_{(a)}^{(k)}$ are the Lagrange multipliers for equality and inequality constraints; and $\eta_{\mathrm{H}(a)}$ is a decision variable to characterize the local optimal cost.

4) S4: denote the optimal solution of (9) as $\boldsymbol{h}_{\mathrm{C}}^{(k)}$, $\boldsymbol{h}_{\mathrm{H}(a)}^{(k)}$, and $\boldsymbol{x}_{\mathrm{H}(a)}^{(k)}$. Some rows in the constraints of (9) are active at the optimal solution, while others remain inactive. Define active constraints by Lagrange multipliers and inactive constraints by their values [24]. To be specific, Lagrange multipliers corresponding to active constraints at the optimal solution is greater than or equal to 0. Residuals corresponding to inactive constraints at the optimal solution are negative.

$$\begin{cases} \left\{\boldsymbol{G}_{\mathrm{C}(a)}^{\mathrm{FC}(k)}\right\}_A\boldsymbol{h}'_{\mathrm{C}}+\left\{\boldsymbol{G}_{\mathrm{H}(a)}^{\mathrm{FC}(k)}\right\}_A\boldsymbol{h}_{\mathrm{H}(a)}^{(k)}=\left\{\boldsymbol{g}_{(a)}^{\mathrm{FC}(k)}\right\}_A \\ \left\{\boldsymbol{\mu}_{(a)}^{(k)}\right\}_A\ge 0 \end{cases} \tag{10}$$

$$\begin{cases} \left\{\boldsymbol{G}_{\mathrm{C}(a)}^{\mathrm{FC}(k)}\right\}_I\boldsymbol{h}'_{\mathrm{C}}+\left\{\boldsymbol{G}_{\mathrm{H}(a)}^{\mathrm{FC}(k)}\right\}_I\boldsymbol{h}_{\mathrm{H}(a)}^{(k)}<\left\{\boldsymbol{g}_{(a)}^{\mathrm{FC}(k)}\right\}_I \\ \left\{\boldsymbol{\mu}_{(a)}^{(k)}\right\}_I=0 \end{cases} \tag{11}$$

where $\{\cdot\}_A$ represents the variables corresponding to active constraints; and $\{\cdot\}_I$ represents the variables corresponding to inactive constraints.

5) S5: subproblem (9) has the following Lagrange formula:

$$\begin{aligned} &\boldsymbol{L}\left(\boldsymbol{h}'_{\mathrm{C}},\boldsymbol{h}_{\mathrm{H}(a)}^{(k)},\boldsymbol{x}_{\mathrm{H}(a)}^{(k)},\boldsymbol{\beta}_{(a)}^{(k)},\boldsymbol{\lambda}_{(a)}^{(k)},\boldsymbol{\mu}_{(a)}^{(k)}\right)=C_{\mathrm{H}(a)}\left(\boldsymbol{h}_{\mathrm{H}(a)}^{(k)}\right)+\left(\boldsymbol{\beta}_{(a)}^{(k)}\right)^{\mathrm{T}}\cdot \\ &\left(\boldsymbol{h}'_{\mathrm{C}}-\boldsymbol{h}_{\mathrm{C}}^{(k)}\right)+\left(\boldsymbol{\lambda}_{(a)}^{(k)}\right)^{\mathrm{T}}\left(\boldsymbol{F}_{\mathrm{C}(a)}\boldsymbol{h}'_{\mathrm{C}}+\boldsymbol{F}_{\mathrm{H}(a)}\boldsymbol{h}_{\mathrm{H}(a)}^{(k)}+\boldsymbol{D}_{\mathrm{H}(a)}\boldsymbol{x}_{\mathrm{H}(a)}^{(k)}-\boldsymbol{f}_{\mathrm{H}(a)}\right)+ \\ &\left\{\boldsymbol{\mu}_{(a)}^{(k)}\right\}_A^{\mathrm{T}}\left(\left\{\boldsymbol{G}_{\mathrm{C}(a)}^{\mathrm{FC}(k)}\right\}_A\boldsymbol{h}'_{\mathrm{C}}+\left\{\boldsymbol{G}_{\mathrm{H}(a)}^{\mathrm{FC}(k)}\right\}_A\boldsymbol{h}_{\mathrm{H}(a)}^{(k)}-\left\{\boldsymbol{g}_{(a)}^{\mathrm{FC}(k)}\right\}_A\right) \end{aligned} \tag{12}$$

The Karush-Kuhn-Tucker conditions for subproblem (9) are as follow.

$$\begin{bmatrix} \boldsymbol{I} & \boldsymbol{0} & \boldsymbol{0} & \boldsymbol{0} & \boldsymbol{0} & \boldsymbol{0} \\ \boldsymbol{F}_{\mathrm{C}(a)}^{(k)} & \boldsymbol{D}_{\mathrm{H}(a)}^{(k)} & \boldsymbol{F}_{\mathrm{H}(a)}^{(k)} & \boldsymbol{0} & \boldsymbol{0} & \boldsymbol{0} \\ \left\{\boldsymbol{G}_{\mathrm{C}(a)}^{\mathrm{FC}(k)}\right\}_A & \boldsymbol{0} & \left\{\boldsymbol{G}_{\mathrm{H}(a)}^{\mathrm{FC}(k)}\right\}_A & \boldsymbol{0} & \boldsymbol{0} & \boldsymbol{0} \\ \boldsymbol{0} & \boldsymbol{0} & \boldsymbol{0} & \boldsymbol{I} & \left(\boldsymbol{F}_{\mathrm{C}(a)}^{(k)}\right)^{\mathrm{T}} & \left\{\boldsymbol{G}_{\mathrm{C}(a)}^{\mathrm{FC}(k)}\right\}_A^{\mathrm{T}} \\ \boldsymbol{0} & \boldsymbol{0} & \boldsymbol{0} & \boldsymbol{0} & \left(\boldsymbol{D}_{\mathrm{H}(a)}^{(k)}\right)^{\mathrm{T}} & \boldsymbol{0} \\ \boldsymbol{0} & \boldsymbol{0} & \boldsymbol{0} & \boldsymbol{0} & \left(\boldsymbol{F}_{\mathrm{H}(a)}^{(k)}\right)^{\mathrm{T}} & \left\{\boldsymbol{G}_{\mathrm{H}(a)}^{\mathrm{FC}(k)}\right\}_A^{\mathrm{T}} \end{bmatrix}\begin{bmatrix} \boldsymbol{h}'_{\mathrm{C}} \\ \boldsymbol{x}_{\mathrm{H}(a)}^{(k)} \\ \boldsymbol{h}_{\mathrm{H}(a)}^{(k)} \\ \boldsymbol{\beta}_{(a)}^{(k)} \\ \boldsymbol{\lambda}_{(a)}^{(k)} \\ \left\{\boldsymbol{\mu}_{(a)}^{(k)}\right\}_A \end{bmatrix}=\begin{bmatrix} \boldsymbol{h}_{\mathrm{C}}^{(k)} \\ \boldsymbol{f}_{\mathrm{H}(a)}^{(k)} \\ \left\{\boldsymbol{g}_{(a)}^{\mathrm{FC}(k)}\right\}_A \\ \boldsymbol{0} \\ \boldsymbol{0} \\ -\boldsymbol{d}_{(a)} \end{bmatrix} \tag{13}$$

where $\boldsymbol{d}_{(a)}$ is a constant vector; and $\boldsymbol{I}$ is an identity matrix.

The following solutions are obtained by solving (13):

$$\begin{bmatrix} \boldsymbol{h}'_{\mathrm{C}} \\ \boldsymbol{x}^{(k)}_{\mathrm{H}(a)} \\ \boldsymbol{h}^{(k)}_{\mathrm{H}(a)} \\ \boldsymbol{\beta}^{(k)}_{(a)} \\ \boldsymbol{\lambda}^{(k)}_{(a)} \\ \left\{\boldsymbol{\mu}^{(k)}_{(a)}\right\}_A \end{bmatrix} = \begin{bmatrix} \boldsymbol{\omega}^{(k)}_{11(a)} & \boldsymbol{\omega}^{(k)}_{12(a)} & \boldsymbol{\omega}^{(k)}_{13(a)} & \boldsymbol{\omega}^{(k)}_{14(a)} & \boldsymbol{\omega}^{(k)}_{15(a)} & \boldsymbol{\omega}^{(k)}_{16(a)} \\ \boldsymbol{\omega}^{(k)}_{21(a)} & \boldsymbol{\omega}^{(k)}_{22(a)} & \boldsymbol{\omega}^{(k)}_{23(a)} & \boldsymbol{\omega}^{(k)}_{24(a)} & \boldsymbol{\omega}^{(k)}_{25(a)} & \boldsymbol{\omega}^{(k)}_{26(a)} \\ \boldsymbol{\omega}^{(k)}_{31(a)} & \boldsymbol{\omega}^{(k)}_{32(a)} & \boldsymbol{\omega}^{(k)}_{33(a)} & \boldsymbol{\omega}^{(k)}_{34(a)} & \boldsymbol{\omega}^{(k)}_{35(a)} & \boldsymbol{\omega}^{(k)}_{36(a)} \\ \boldsymbol{\omega}^{(k)}_{41(a)} & \boldsymbol{\omega}^{(k)}_{42(a)} & \boldsymbol{\omega}^{(k)}_{43(a)} & \boldsymbol{\omega}^{(k)}_{44(a)} & \boldsymbol{\omega}^{(k)}_{45(a)} & \boldsymbol{\omega}^{(k)}_{46(a)} \\ \boldsymbol{\omega}^{(k)}_{51(a)} & \boldsymbol{\omega}^{(k)}_{52(a)} & \boldsymbol{\omega}^{(k)}_{53(a)} & \boldsymbol{\omega}^{(k)}_{54(a)} & \boldsymbol{\omega}^{(k)}_{55(a)} & \boldsymbol{\omega}^{(k)}_{56(a)} \\ \boldsymbol{\omega}^{(k)}_{61(a)} & \boldsymbol{\omega}^{(k)}_{62(a)} & \boldsymbol{\omega}^{(k)}_{63(a)} & \boldsymbol{\omega}^{(k)}_{64(a)} & \boldsymbol{\omega}^{(k)}_{65(a)} & \boldsymbol{\omega}^{(k)}_{66(a)} \end{bmatrix} \begin{bmatrix} \boldsymbol{h}^{(k)}_{\mathrm{C}} \\ \boldsymbol{f}^{(k)}_{\mathrm{H}(a)} \\ \left\{\boldsymbol{g}^{\mathrm{FC}(k)}_{(a)}\right\}_A \\ \boldsymbol{0} \\ \boldsymbol{0} \\ -\boldsymbol{d}_{(a)} \end{bmatrix} \tag{14}$$

where $\boldsymbol{\omega}^{(k)}_{ij(a)}$ is the block matrix element of the i^{th} row and the j^{th} column of the a^{th} DHN in the k^{th} iteration.

$\boldsymbol{h}^{(k)}_{\mathrm{H}(a)}$ is an affine function of boundary variables $\boldsymbol{h}^{(k)}_{\mathrm{C}}$.

$$\boldsymbol{h}^{(k)}_{\mathrm{H}(a)} = \varphi_{(a)}\left(\boldsymbol{h}^{(k)}_{\mathrm{C}}\right) = \boldsymbol{\omega}^{(k)}_{31(a)}\boldsymbol{h}^{(k)}_{\mathrm{C}} + \boldsymbol{\omega}^{(k)}_{32(a)}\boldsymbol{f}^{(k)}_{\mathrm{H}(a)} + \boldsymbol{\omega}^{(k)}_{33(a)}\left\{\boldsymbol{g}^{\mathrm{FC}(k)}_{(a)}\right\}_A - \boldsymbol{\omega}^{(k)}_{36(a)}\boldsymbol{d}_{(a)} \tag{15}$$

where $\varphi_{(a)}(\cdot)$ is the affine function.

Taking the boundary variables $\boldsymbol{h}^{(k)}_{\mathrm{C}}$ as parameters, the local optimal cost is expressed as:

$$LOC^{(k)}_{(a)}\left(\boldsymbol{h}^{(k)}_{\mathrm{C}}\right) = \boldsymbol{d}^{\mathrm{T}}_{(a)}\varphi_{(a)}\left(\boldsymbol{h}^{(k)}_{\mathrm{C}}\right) + e_{(a)} \tag{16}$$

where $e_{(a)}$ is a constant.

For active constraints, Lagrange multipliers $\left\{\boldsymbol{\mu}^{(k)}_{(a)}\right\}_A$ are an affine function of $\boldsymbol{h}^{(k)}_{\mathrm{C}}$.

$$\left\{\boldsymbol{\mu}^{(k)}_{(a)}\right\}_A = \boldsymbol{\omega}^{(k)}_{61(a)}\boldsymbol{h}^{(k)}_{\mathrm{C}} + \boldsymbol{\omega}^{(k)}_{62(a)}\boldsymbol{f}^{(k)}_{\mathrm{H}(a)} + \boldsymbol{\omega}^{(k)}_{63(a)}\left\{\boldsymbol{g}^{\mathrm{FC}(k)}_{(a)}\right\}_A - \boldsymbol{\omega}^{(k)}_{66(a)}\boldsymbol{d}_{(a)} \geq \boldsymbol{0} \tag{17}$$

By substituting (15) to inactive constraints, we can obtain:

$$\left\{\boldsymbol{G}^{\mathrm{FC}(k)}_{\mathrm{H}(a)}\right\}_I\left(\boldsymbol{\omega}^{(k)}_{32(a)}\boldsymbol{f}^{(k)}_{\mathrm{H}(a)} + \boldsymbol{\omega}^{(k)}_{33(a)}\left\{\boldsymbol{g}^{\mathrm{FC}(k)}_{(a)}\right\}_A - \boldsymbol{\omega}^{(k)}_{36(a)}\boldsymbol{d}_{(a)}\right) + \left(\left\{\boldsymbol{G}^{\mathrm{FC}(k)}_{\mathrm{C}(a)}\right\}_I + \left\{\boldsymbol{G}^{\mathrm{FC}(k)}_{\mathrm{H}(a)}\right\}_I\boldsymbol{\omega}^{(k)}_{31(a)}\right)\boldsymbol{h}^{(k)}_{\mathrm{C}} \leq \left\{\boldsymbol{g}^{\mathrm{FC}(k)}_{(a)}\right\}_I \tag{18}$$

Both (17) and (18) are some half-planes from a geometric point of view with respect to the parameter $\boldsymbol{h}^{(k)}_{\mathrm{C}}$, which define the critical region in the a^{th} DHN during the k^{th} iteration, written as $CR^{(k)}_{(a)}$. Each DHN sends $CR^{(k)}_{(a)}$ and $LOC^{(k)}_{(a)}\left(\boldsymbol{h}^{(k)}_{\mathrm{C}}\right)$ to EPN.

6) S6: EPN collects $CR^{(k)}_{(a)}$ and $LOC^{(k)}_{(a)}\left(\boldsymbol{h}^{(k)}_{\mathrm{C}}\right)$ for all DHN subproblems. The augmented improved master problem is expressed as:

$$\begin{cases} \left(\boldsymbol{x}^{(k+1)}_{\mathrm{E}}, \boldsymbol{h}^{(k+1)}_{\mathrm{C}}, \boldsymbol{h}^{(k+1)}_{\mathrm{H}(a)}, \eta^{(k+1)}_{(a)}\right) = \underset{\boldsymbol{x}_{\mathrm{E}}, \boldsymbol{h}_{\mathrm{C}}, \boldsymbol{h}_{\mathrm{H}(a)}, \eta_{(a)}}{\arg\min} \left\{C_{\mathrm{E}}(\boldsymbol{x}_{\mathrm{E}}, \boldsymbol{h}_{\mathrm{C}}) + \sum_{a=1}^{n}\eta_{(a)}\right\} \\ \text{s.t. } \boldsymbol{D}_{\mathrm{E}}\boldsymbol{x}_{\mathrm{E}} + \boldsymbol{B}_{\mathrm{C}}\boldsymbol{h}_{\mathrm{C}} \leq \boldsymbol{b}_{\mathrm{E}} \\ \quad \boldsymbol{G}^{\mathrm{FC}}_{\mathrm{C}(a)}\boldsymbol{h}_{\mathrm{C}} + \boldsymbol{G}^{\mathrm{FC}}_{\mathrm{H}(a)}\boldsymbol{h}'_{\mathrm{H}(a)} \leq \boldsymbol{g}^{\mathrm{FC}}_{(a)} \\ \quad \boldsymbol{h}_{\mathrm{C}} \in CR_{(a)} \\ \quad \eta_{(a)} \geq LOC_{(a)}\left(\boldsymbol{h}_{\mathrm{C}}\right) \\ \quad a = 1, 2, \ldots, n \end{cases} \tag{19}$$

7) S7: EPN solves the augmented improved master problem (19) and checks whether the local optimal costs in the two adjacent critical regions are equal. The local optimal costs in the two adjacent critical regions are strictly equal in theory. However, there is an error in the numerical simulation, so we test if the local optimal costs in the two adjacent critical regions are equal by setting δ to be 0.5. If $\left|LOC^{(k)}_{(a)}\left(\boldsymbol{h}^{(k)}_{\mathrm{C}}\right) - LOC^{(k-1)}_{(a)}\left(\boldsymbol{h}^{(k)}_{\mathrm{C}}\right)\right| > \delta$, the local optimal cost in the two adjacent critical regions is not equal in the k^{th} iteration. In other words, the a^{th} DHN modifies its local optimal cost in the k^{th} iteration. Thus, the a^{th} DHN is dishonest, and it is dispatched separately. The EPN and other honest DHNs form a coalition. They are dispatched in a coordinated manner.

8) S8: calculate the optimal value $y^{(k)}$. ε is the convergence parameter and is equal to 0.01. If $\left|y^{(k)} - y^{(k-1)}\right| < \varepsilon$, terminate the iteration. Update $k := k+1$ and go to S3, otherwise.

In summary, EPN transfers the heat output of CHP units, denoted as $\boldsymbol{h}_{\mathrm{C}}$, to DHN first. In particular, $\boldsymbol{h}_{\mathrm{C}}$ is not only a boundary coupling variable, but also a parameter in multiparameter programming theory. Next, DHN transmits critical region and local optimal cost to ENP. Finally, EPN compares the collected *LOC* based on corollary to identify fraudulent information. A flowchart of the distributed algorithm with fraud detection is shown in Fig. 4.

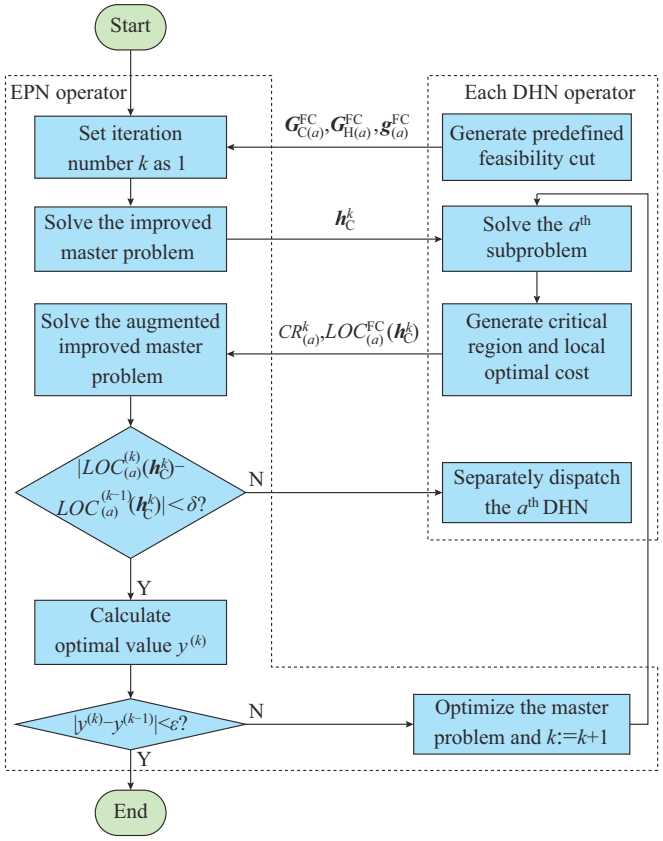

Fig. 4. Flowchart of distributed algorithm with fraud detection.

IV. Fair Benefit Distribution Mechanism of Coalition

The fraud detection method selects honest entities to form a coalition. Entities in the coalition are dispatched coordinately, while dishonest entities are dispatched separately. Combined dispatch of IEHSs reduces coalition cost due to cooperative surplus but leads to higher cost for DHNs. Without a fair benefit distribution mechanism, DHNs have no incentive to cooperate with EPNs.

In this section, we prepare to allocate cooperative surplus by calculating the Shapley value based on the marginal contribution of each entity. The cooperative game emphasizes collective rationality and pursues the maximization of collective interests. Fair distribution of cooperative surplus is a prerequisite for effective cooperation. Given a coalitional game $G=\langle N, v\rangle, |N|=n$, the Shapley value of player i is defined as [25]:

$$\varphi_i(G)=\frac{1}{n!}\sum_{S\subseteq N\setminus\{i\}}|S|!(n-|S|-1)!\left[v(S\cup\{i\})-v(S)\right] \quad (20)$$

where N is a universal set including n players; S is a subset excluding player i; $|S|$ is the number of players in set S; and $v(S)$ is a characteristic function representing the sum of the total expected payoffs that the players in set S can obtain by cooperation.

The basic idea of the Shapley value is that players reasonably expect to be paid for their marginal contribution. Since EPN and DHN are operated by different entities, it is not practical to calculate Shapley values centrally. Benders decomposition preserves the privacy of different entities in IEHS dispatch, which paves the way for calculating Shapley values in a distributed manner.

There are one EPN and n DHNs in IEHS dispatch. Assume that E denotes the EPN and H_i denotes the i^{th} DHN. The universal set is $N=\{E, H_1, H_2, \ldots, H_n\}$. The subsets include $\{E, H_1\}, \{E, H_1, H_2\}, \ldots, \{E, H_1, H_2, \ldots, H_{n-1}\}$ and so on. Each subset maps a characteristic function $v(S)$. For ease of understanding, we take the cooperation between one EPN and one DHN as an example. In this case, the universal set is $N=\{E, H\}$. The subsets of EPN include $S_{E1}=\{E\}$ and $S_{E2}=\{E, H\}$. The subsets of DHN include $S_{H1}=\{H\}$ and $S_{H2}=\{E, H\}$.

C'_E and C'_H denote the costs of EPN and DHN in separated dispatch. They are mapped to $v(S_{E1})$ and $v(S_{H1})$, respectively. C_{IEHS} denotes the overall cost of IEHS in combined dispatch, and it is mapped to $v(S_{E2})$ or $v(S_{H2})$. In order to ensure incentive compatibility among all players, we recalculate the costs of EPN and DHN based on Shapley values by (20). For example, $C^S_E=(C_{IEHS}+C'_E-C'_H)/2$ and $C^S_H=(C_{IEHS}+C'_H-C'_E)/2$ denote the costs of EPN and DHN in combined dispatch after calculating Shapley values. Likewise, we can calculate Shapley values of multiple entities.

V. Case Study

This section presents two IEHS case studies at different scales. First, the fraud detection method is used to check whether the local optimal costs in the two adjacent critical regions are identical. Specifically, the fraud detection method reveals the authenticity of information exchanged between EPN and DHNs. Moreover, all honest entities are selected to form a coalition. The cooperative surplus generated by the coalition is allocated by calculating Shapley values based on the marginal contribution of each entity. In summary, two case studies highlight fraud detection, privacy protection, and incentive compatibility of the proposed cooperation mechanism with information asymmetry. Simulation tests were performed on a computer with an Intel i7-10700F CPU and 16 GB of RAM. The Gurobi solver [27] in MATLAB was used to solve these problems. Table II shows the scale information of two IEHS case studies. Further details about the data can be found in [28].

TABLE II
Scale Information of Two IEHS Case Studies

Scale	EPN					DHN			
	Bus	Branch	Thermal unit	CHP	Wind unit	Node	Pipeline	Heat boiler	Heat load
Small	6	7	2	2	1	6	5	1	2
Large	319	431	120	20	68	40	35	5	15

A. Small-scale IEHS

Figure 5 shows the diagram of a small-scale IEHS consisting of a 6-bus EPN and a 6-node DHN. Bs stands for bus; G stands for generator; W stands for wind farm; D stands for electrical load; Nd stands for node; HES stands for heat exchange station; and HL stands for heat load. Further details about the data can be found in [28]. The fraud detection process in small-scale IEHS is shown in Table III. The fraud detection method examines local optimal costs in the two adjacent critical regions.

In the first case, DHN does not change the local optimal costs during each iteration. The local optimal costs in the two adjacent critical regions are both \$4604. Similarly, the local optimal costs in the two adjacent critical regions during the second iteration are both \$3607. To be exact, the information exchanged between EPN and DHN is authentic. As a result, EPN and DHN form a coalition and coordinate scheduling.

However, in the second case, the local optimal costs in the two adjacent critical regions during the second iteration are \$3607 and \$3807, respectively. It violates the corollary that local optimal costs in the two adjacent critical regions are equal. DHN operator wants to increase the local optimal costs in the second iteration to get more compensation from EPN, i.e., there is marketing fraud in DHN. Thereby, in the second case, EPN and DHN are dispatched separately.

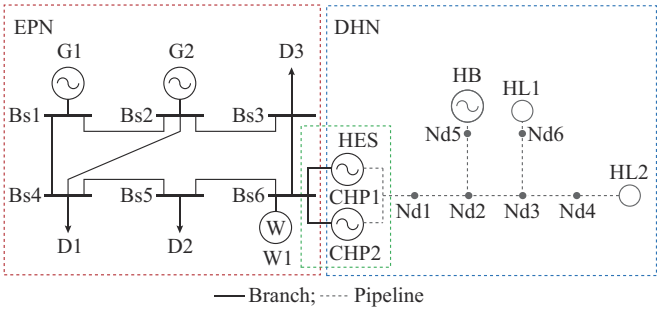

Fig. 5. Diagram of small-scale IEHS.

TABLE III
FRAUD DETECTION PROCESS IN SMALL-SCALE IEHS

k	First case		Second case	
	$LOC^{(k-1)}(\boldsymbol{h}_C^{(k)})$ ($)	$LOC^{(k)}(\boldsymbol{h}_C^{(k)})$ ($)	$LOC^{(k-1)}(\boldsymbol{h}_C^{(k)})$ ($)	$LOC^{(k)}(\boldsymbol{h}_C^{(k)})$ ($)
1	4604	4064	4604	4064
2	3607	3607	3607	3807

Combined dispatch of IEHS can improve the flexibility of EPN. Overall heat output of small-scale IEHS is shown in Fig. 6.

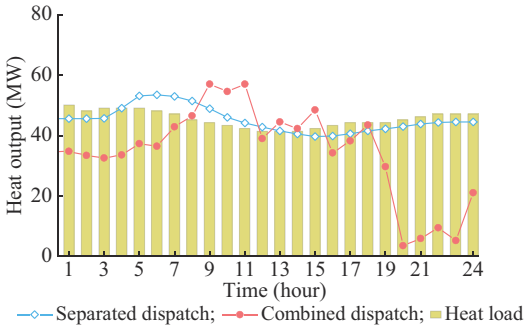

Fig. 6. Overall heat output in small-scale IEHS.

Heat output in separate dispatch almost matches heat loads, whereas DHN is heated earlier during the trough period of heat loads in combined dispatch; at night, CHP units in combined dispatch operate at a low output level. At the same time, relatively more expensive HBs will replace CHP units to provide heat. Accordingly, the use of pipeline heat storage can improve the operational flexibility of EPN, but results in more operating cost and heat losses for DHN.

Combined dispatch of IEHS can reduce wind curtailment. Figure 7 shows the overall wind curtailment in small-scale IEHS.

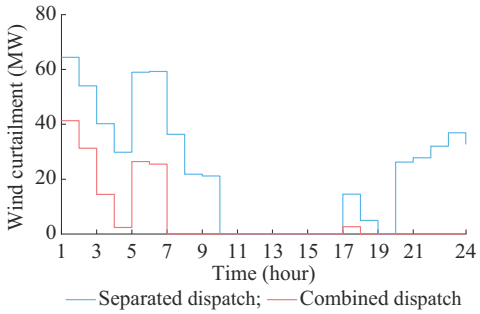

Fig. 7. Overall wind curtailment in small-scale IEHS.

At night, heat loads are high, and CHP units generate enormous electricity while producing heat, so wind power must be reduced. The reduction causes severe wind curtailment in separated dispatch. On the contrary, CHP units in combined dispatch operate at low output at night to free up space for wind utilization.

Table IV summarizes and compares the economic performance of small-scale IEHS. Traditional combined dispatch does not redistribute the benefits of EPN and DHN. To achieve incentive compatibility, we recalculate the cost of EPN and DHN based on Shapley values in combined dispatch.

TABLE IV
ECONOMIC PERFORMANCE OF SMALL-SCALE IEHS

Dispatch model	EPN				DHN		Total cost of IEHS ($)
	Wind curtailment penalty ($)	Thermal cost ($)	CHP cost ($)	Overall cost ($)	HB cost ($)	Overall cost ($)	
Separated dispatch	23084	82664	14690	120438	900	900	121338
Combined dispatch (traditional)	5923	82718	12968	101609	1857	1857	103466
Combined dispatch (Shapley)				111502		−8036	103466

Combined dispatch reduces wind curtailment by 74.3% compared with the separate dispatch. The total cost of IEHS in combined dispatch is $17872 less than the separated dispatch. The cost of EPN in the combined dispatch is $18829 less than in the separated dispatch. Nevertheless, the cost of DHN in the combined dispatch is $957 more than in the separated dispatch. In short, the cost of EPN decreases and the cost of DHN increases after cooperation.

To promote cooperation, we calculate Shapley values based on the marginal contribution of each entity to fairly distribute the cooperative surplus generated by the coalition. Calculation of Shapley values shows that cost of EPN is $111502. Specifically, EPN awards DHN $9893 as compensation. The cost of DHN is $−8036. In other words, the total payoffs of DHN are $8036. Total cost of IEHS in combined dispatch remains $17872. Both EPN and DHN benefit from the cooperation that ensures incentive compatibility.

B. Large-scale IEHS

We further verify fraud detection, privacy protection, and incentive compatibility of the proposed cooperation mechanism with information asymmetry in large-scale IEHS.

We first check whether the local optimal costs in two adjacent critical regions of all DHNs are equal. The fraud detection process in large-scale IEHS is presented in Table V. The local optimal costs in two adjacent critical regions of DHN1, DHN2, and DHN3 are equal. Thus, DHN1, DHN2, and DHN3 do not modify the operating cost of HBs during each iteration. The information exchanged between EPN and DHN1, DHN2, and DHN3 is authentic. Through the fraud detection method, EPN, DHN1, DHN2, and DHN3 are selected as honest entities. In addition, EPN, DHN1, DHN2, and DHN3 form a coalition $S=\{\mathrm{E}, \mathrm{H}_1, \mathrm{H}_2, \mathrm{H}_3\}$. The players in the coalition are dispatched coordinately.

EPN and DHNs belonging to different entities under asymmetric information may result in marketing fraud. In contrast, local optimal costs in two adjacent critical regions of DHN4 are not equal in the 10th iteration. The local optimal costs in two adjacent critical regions of DHN5 are not equal in the 7th iteration. DHN4 and DHN5 increase the operating cost of HBs to obtain more compensation. Therefore, DHN4 and DHN5 are dishonest players and are dispatched separately.

TABLE V
FRAUD DETECTION PROCESS IN LARGE-SCALE IEHS

k	DHN1		DHN2		DHN3		DHN4		DHN5	
	$LOC_{(1)}^{(k-1)}\left(\boldsymbol{h}_{\mathrm{C}}^{(k)}\right)$ ($)	$LOC_{(1)}^{(k)}\left(\boldsymbol{h}_{\mathrm{C}}^{(k)}\right)$ ($)	$LOC_{(2)}^{(k-1)}\left(\boldsymbol{h}_{\mathrm{C}}^{(k)}\right)$ ($)	$LOC_{(2)}^{(k)}\left(\boldsymbol{h}_{\mathrm{C}}^{(k)}\right)$ ($)	$LOC_{(3)}^{(k-1)}\left(\boldsymbol{h}_{\mathrm{C}}^{(k)}\right)$ ($)	$LOC_{(3)}^{(k)}\left(\boldsymbol{h}_{\mathrm{C}}^{(k)}\right)$ ($)	$LOC_{(4)}^{(k-1)}\left(\boldsymbol{h}_{\mathrm{C}}^{(k)}\right)$ ($)	$LOC_{(4)}^{(k)}\left(\boldsymbol{h}_{\mathrm{C}}^{(k)}\right)$ ($)	$LOC_{(5)}^{(k)}\left(\boldsymbol{h}_{\mathrm{C}}^{(k)}\right)$ ($)	$LOC_{(5)}^{(k-1)}\left(\boldsymbol{h}_{\mathrm{C}}^{(k)}\right)$ ($)
1	2405	2405	2405	2405	2405	2405	2405	2405	2435	2435
2	2369	2369	2368	2368	2369	2369	2361	2361	2365	2365
3	2332	2332	2331	2331	2297	2297	2286	2286	2311	2311
4	2278	2278	2313	2313	2260	2260	2229	2229	2275	2275
5	2241	2241	2295	2295	2224	2224	2193	2193	2257	2257
6	2188	2188	2277	2277	2152	2152	2139	2139	2239	2239
7	2134	2134	2259	2259	2133	2133	2121	2121	2221	2235
8	2116	2116	2242	2242	2116	2116	2103	2103	2203	2203
9	2098	2098	2226	2226	2098	2098	2085	2085	2203	2203
10	2080	2080	2206	2206	2080	2080	2067	2080	2203	2203
11	2079	2079	2188	2188	2062	2062	2049	2049	2203	2203
12	2062	2062	2170	2170	2044	2044	2048	2048	2203	2203
13	2044	2044	2152	2152	2025	2025	2048	2048	2203	2203
14	2025	2025	2134	2134	2025	2025	2048	2048	2203	2203
15	2025	2025	2115	2115	2025	2025	2048	2048	2203	2203

A summary and comparison of the economic performance of large-scale IEHS are shown in Table VI. Traditional combined dispatch does not redistribute the benefits of EPN and DHNs. Additionally, we calculated the cost of EPN and DHNs based on Shapley values in a combined dispatch to ensure incentive compatibility.

TABLE VI
ECONOMIC PERFORMANCE OF LARGE-SCALE IEHS

Dispatch model	EPN				DHN1		DHN2		DHN3		DHN4		DHN5		Total cost of IEHS ($)
	Wind curtailment penalty ($)	Thermal cost ($)	CHP cost ($)	Overall cost ($)	HB cost ($)	Overall cost ($)	HB cost ($)	Overall cost ($)	HB cost ($)	Overall cost ($)	HB cost ($)	Overall cost ($)	HB cost ($)	Overall cost ($)	
Separated dispatch	5168	69551	113244	187963.00	1976	1976	1976	1976.00	1976	1976.00	1976	1976	1976	1976	197843
Combined dispatch (traditional)	5117	69546	113034	187697.00	2025	2025	1989	1989.00	2025	2025.00	1976	1976	1976	1976	197688
Combined dispatch (Shapley)				187899.17		1933		1951.67		1952.17		1976		1976	197688

The total cost of IEHS in separated dispatch is \$197843. The cost of EPN in the coalition S_3 is \$266 less than the separated dispatch. The cost of DHN1 in the coalition S_3 is \$49 more than the separated dispatch. The cost of DHN2 in the coalition S_3 is \$13 more than the separated dispatch. The cost of DHN3 in the coalition S_3 is \$49 more than the separated dispatch. In brief, the cost of EPN decreases, while the costs of DHN1, DHN2, and DHN3 in the coalition S_3 increase.

If DHN transmits fake information to EPN, this behavior can be identified through the fraud detection method. EPN and DHN do not form a coalition, so they are dispatched separately. If lying does not benefit players, they will not lie. Based on the rational perspective, EPN and DHN will exchange authentic information to form a stable coalition. In summary, the proposed mechanism stimulates cooperation while achieving Pareto optimality under asymmetric information.

VI. Conclusion

In this paper, we propose a cooperation mechanism design for IEHS with information asymmetry. The basic idea is to bridge the gap between optimal scheduling of IEHS and information asymmetry among multiple entities. Fraud detection, privacy protection, and incentive compatibility are all included in the proposed mechanism. The proposed fraud detection method based on multiparametric programming with guaranteed feasibility reveals the authenticity of the information exchanged between EPNs and DHNs. It overcomes information asymmetry among multiple entities. All honest entities are selected to form a coalition and coordinate scheduling, while dishonest entities submitting false information are dispatched separately. Moreover, to protect private information and distribute benefits fairly, Shapley values of the coalition are calculated in a distributed manner through enhanced Benders decomposition. The coalition as a whole achieves incentive compatibility. In particular, the designed mechanism encourages cooperation while achieving Pareto optimality under asymmetric information. In the future, we plan to design a cooperation mechanism for IEHS that considers information asymmetry and uncertainty.

Appendix A

A. DHN Model

The main components of a typical DHN are heat generation sources, primary and secondary networks, heat stations, and heat loads [29]. Primary and secondary networks in DHN are analogous to transmission and distribution networks in EPN. Heat is transported from heat sources to heat stations through primary networks. Heat stations transfer heat to consumers through secondary networks. Secondary networks are not only exceedingly complex in topology, but also have few accessible measurements. As a result, only primary networks are modeled in this paper. Heat stations correspond to heat loads. The simplified DHN includes sources, loads, and primary networks. In this paper, the expression is simplified by summarizing the variables into vectors.

1) Heat Generation Source

CHP units dispatched by EPN operators and HBs controlled by DHN operators make up heat generation sources:

$$\boldsymbol{h}=[\boldsymbol{h}_{\mathrm{C}}\quad \boldsymbol{h}_{\mathrm{H}}]=c\boldsymbol{M}^{\mathrm{G}}\left(\boldsymbol{\tau}^{\mathrm{GS}}-\boldsymbol{\tau}^{\mathrm{GR}}\right) \tag{A1}$$

where $\boldsymbol{h}$ is the total heat output; $\boldsymbol{h}_{\mathrm{C}}$ is the heat output supplied by CHP units; $\boldsymbol{h}_{\mathrm{H}}$ is the heat output supplied by HBs; $\boldsymbol{\tau}^{\mathrm{GS}}$ is the supply temperature of heat sources; $\boldsymbol{\tau}^{\mathrm{GR}}$ is the return temperature of heat sources; $\boldsymbol{M}^{\mathrm{G}}$ is the mass flow rate matrix of heat sources; and c is the heat capacity of water.

The operating cost of HBs in the a^{th} DHN is a linear function:

$$C_{\mathrm{H}(a)}\left(\boldsymbol{h}_{\mathrm{H}(a)}\right)=\boldsymbol{d}_{(a)}^{\mathrm{T}}\boldsymbol{h}_{\mathrm{H}(a)}+e_{(a)} \tag{A2}$$

$\boldsymbol{h}_{\mathrm{H}(a)}$ should adhere to operating limits:

$$\underline{\boldsymbol{h}}_{\mathrm{H}(a)}\le\boldsymbol{h}_{\mathrm{H}(a)}\le\bar{\boldsymbol{h}}_{\mathrm{H}(a)} \tag{A3}$$

where $\underline{\boldsymbol{h}}_{\mathrm{H}(a)}$ and $\bar{\boldsymbol{h}}_{\mathrm{H}(a)}$ are the lower and upper limits of heat generation supplied by HBs in the a^{th} DHN, respectively.

2) Thermal Dynamics

The nodal method characterizes thermal dynamics in this paper. It mainly includes transfer delays and heat losses. The outlet temperature of pipelines is estimated by neglecting heat losses:

$$\boldsymbol{\tau}'^{\mathrm{PS,out}}=\boldsymbol{Q}\boldsymbol{\tau}^{\mathrm{PS,in}}+\hat{\boldsymbol{\tau}}^{\mathrm{PS,out}} \tag{A4}$$

$$\boldsymbol{\tau}'^{\mathrm{PR,out}}=\boldsymbol{Q}\boldsymbol{\tau}^{\mathrm{PR,in}}+\hat{\boldsymbol{\tau}}^{\mathrm{PR,out}} \tag{A5}$$

where $\boldsymbol{\tau}'^{\mathrm{PS,out}}$ and $\boldsymbol{\tau}'^{\mathrm{PR,out}}$ are the outlet temperatures influenced by the historical inlet temperature of the supply and return pipelines in past periods, respectively; $\hat{\boldsymbol{\tau}}^{\mathrm{PS,out}}$ and $\hat{\boldsymbol{\tau}}^{\mathrm{PR,out}}$ are the residue temperatures; $\boldsymbol{\tau}^{\mathrm{PS,in}}$ and $\boldsymbol{\tau}^{\mathrm{PR,in}}$ are the mass flow temperatures at pipeline inlet in the supply and return networks, respectively; and $\boldsymbol{Q}$ is the transfer delay coefficient matrix.

Considering heat losses, outlet temperatures are revised as:

$$\boldsymbol{\tau}^{\mathrm{PS,out}}=\hat{\boldsymbol{\tau}}^{\mathrm{A}}+\boldsymbol{\lambda}(\boldsymbol{\tau}'^{\mathrm{PS,out}}-\hat{\boldsymbol{\tau}}^{\mathrm{A}}) \tag{A6}$$

$$\boldsymbol{\tau}^{\mathrm{PR,out}}=\hat{\boldsymbol{\tau}}^{\mathrm{A}}+\boldsymbol{\lambda}(\boldsymbol{\tau}'^{\mathrm{PR,out}}-\hat{\boldsymbol{\tau}}^{\mathrm{A}}) \tag{A7}$$

where $\boldsymbol{\lambda}$ is the heat-loss factor coefficient matrix; and $\hat{\boldsymbol{\tau}}^{\mathrm{A}}$ is ambient temperature.

3) Law of Temperature Mixing

Mass flow at nodes is mixed by the following equations to determine the node temperature:

$$\boldsymbol{A}_{-}\otimes\boldsymbol{I}_{\mathrm{T}}\cdot\boldsymbol{\Omega}^{\mathrm{PS}}\boldsymbol{\tau}^{\mathrm{PS,out}}+\boldsymbol{A}_{\mathrm{G}}\otimes\boldsymbol{I}_{\mathrm{T}}\cdot\boldsymbol{\Omega}^{\mathrm{GS}}\boldsymbol{\tau}^{\mathrm{GS}}=\boldsymbol{\tau}^{\mathrm{NS}} \tag{A8}$$

$$\boldsymbol{A}_{+}\otimes\boldsymbol{I}_{\mathrm{T}}\cdot\boldsymbol{\Omega}^{\mathrm{PR}}\boldsymbol{\tau}^{\mathrm{PR,out}}+\boldsymbol{A}_{\mathrm{D}}\otimes\boldsymbol{I}_{\mathrm{T}}\cdot\boldsymbol{\Omega}^{\mathrm{DR}}\boldsymbol{\tau}^{\mathrm{DR}}=\boldsymbol{\tau}^{\mathrm{NR}} \tag{A9}$$

where $\boldsymbol{A}_{\mathrm{G}}$ and $\boldsymbol{A}_{\mathrm{D}}$ are the node-source incidence matrices and node-load incidence matrices, respectively; $\boldsymbol{A}_{+}=\max(\boldsymbol{A},0)$ and $\boldsymbol{A}_{-}=\max(-\boldsymbol{A},0)$ represent the downstream pipelines and upstream pipelines in supply networks, respectively; $\boldsymbol{\Omega}^{\mathrm{PS}}$, $\boldsymbol{\Omega}^{\mathrm{PR}}$, $\boldsymbol{\Omega}^{\mathrm{GS}}$, and $\boldsymbol{\Omega}^{\mathrm{GR}}$ are mass factor matrices; $\boldsymbol{I}_{\mathrm{T}}$ is the identity matrix; $\boldsymbol{\tau}^{\mathrm{DR}}$ is the return temperature of heat loads; $\boldsymbol{\tau}^{\mathrm{NS}}$ and $\boldsymbol{\tau}^{\mathrm{NR}}$ are the mixed temperatures of supply and return networks, respectively; and $\boldsymbol{\tau}^{\mathrm{PS,out}}$ and $\boldsymbol{\tau}^{\mathrm{PR,out}}$ are the mass flow temperatures taking into account temperature drop.

4) Inlet Temperature

Using the well-known node-branch incidence matrix $\boldsymbol{A}$ and the mass flow direction in supply networks as the reference direction, the topology is described as:

$$\boldsymbol{A}=\left(a_{ib}\right)_{N\times M} \tag{A10}$$

$$a_{ib}=\begin{cases}1 & b\in\mathcal{P}_i^{+}\\ -1 & b\in\mathcal{P}_i^{-}\\ 0 & \text{otherwise}\end{cases} \tag{A11}$$

where $\mathcal{P}_i^{+}$ is the set of supply/return pipelines starting/ending at node i; $\mathcal{P}_i^{-}$ is the set of supply/return pipelines ending/starting at node i; N is the cardinality of nodes in the DHN; and M is the cardinality of nodes in the EPN. $\boldsymbol{A}$ is divided into the matrices $\boldsymbol{A}_{+}=\max(\boldsymbol{A},0)$ and $\boldsymbol{A}_{-}=\max(-\boldsymbol{A},0)$ to represent downstream pipelines $\mathcal{P}_i^{+}$ and upstream pipelines $\mathcal{P}_i^{-}$ in supply networks, respectively. The topology of return networks is presumed to be same as that of supply networks to simple notations. As a result, $\boldsymbol{A}_{-}$ and $\boldsymbol{A}_{+}$ represent downstream pipelines $\mathcal{P}_i^{-}$ and upstream pipelines $\mathcal{P}_i^{+}$ in return networks, respectively.

The elements of node-source incidence matrix $\boldsymbol{A}_{\mathrm{G}}=$

$\left(a_{ig}^{\mathrm{G}}\right)_{N\times N_{\mathrm{G}}}$ and node-load incidence matrix $\boldsymbol{A}_{\mathrm{D}}=\left(a_{il}^{\mathrm{D}}\right)_{N\times N_{\mathrm{D}}}$ are also defined as follows, and N_{G} and N_{D} are the cardinalities of heat sources and loads, respectively.

$$a_{ig}^{\mathrm{G}}=\begin{cases}1 & g\in\mathcal{G}_i\\ 0 & \text{otherwise}\end{cases} \tag{A12}$$

$$a_{il}^{\mathrm{D}}=\begin{cases}1 & l\in\mathcal{D}_i\\ 0 & \text{otherwise}\end{cases} \tag{A13}$$

where $\mathcal{G}_i$ and $\mathcal{D}_i$ are the sets of heat sources and loads connecting to node i, respectively.

Inlet temperature of pipelines is determined by the temperature of the starting-end node as:

$$\boldsymbol{A}_{\mathrm{D}}^{\mathrm{T}}\otimes\boldsymbol{I}_{\mathrm{T}}\cdot\boldsymbol{\tau}^{\mathrm{NS}}=\boldsymbol{\tau}^{\mathrm{DS}} \tag{A14}$$

$$\boldsymbol{A}_{\mathrm{G}}^{\mathrm{T}}\otimes\boldsymbol{I}_{\mathrm{T}}\cdot\boldsymbol{\tau}^{\mathrm{NR}}=\boldsymbol{\tau}^{\mathrm{GR}} \tag{A15}$$

$$\boldsymbol{A}_{+}^{\mathrm{T}}\otimes\boldsymbol{I}_{\mathrm{T}}\cdot\boldsymbol{\tau}^{\mathrm{NS}}=\boldsymbol{\tau}^{\mathrm{PS,in}} \tag{A16}$$

$$\boldsymbol{A}_{+}^{\mathrm{T}}\otimes\boldsymbol{I}_{\mathrm{T}}\cdot\boldsymbol{\tau}^{\mathrm{NR}}=\boldsymbol{\tau}^{\mathrm{PR,in}} \tag{A17}$$

where $\boldsymbol{\tau}^{\mathrm{DS}}$ is the supply temperature of heat loads.

5) Heat Demand

The heat exchange station is modeled as:

$$\boldsymbol{d}=c\boldsymbol{M}^{\mathrm{D}}\left(\boldsymbol{\tau}^{\mathrm{DS}}-\boldsymbol{\tau}^{\mathrm{DR}}\right) \tag{A18}$$

where $\boldsymbol{d}$ is the matrix of total heat loads; and $\boldsymbol{M}^{\mathrm{D}}$ is the mass flow rate matrix of heat loads.

6) Operating Limits

The state of DHN should remain within operating limits.

$$\underline{\boldsymbol{\tau}}^{\mathrm{NS}}\le\boldsymbol{\tau}^{\mathrm{NS}}\le\bar{\boldsymbol{\tau}}^{\mathrm{NS}} \tag{A19}$$

$$\underline{\boldsymbol{\tau}}^{\mathrm{NR}}\le\boldsymbol{\tau}^{\mathrm{NR}}\le\bar{\boldsymbol{\tau}}^{\mathrm{NR}} \tag{A20}$$

where $\underline{\boldsymbol{\tau}}^{\mathrm{NS}}$ and $\bar{\boldsymbol{\tau}}^{\mathrm{NS}}$ are the lower and upper limits of mixed temperature of supply networks, respectively; and $\underline{\boldsymbol{\tau}}^{\mathrm{NR}}$ and $\bar{\boldsymbol{\tau}}^{\mathrm{NR}}$ are the lower and upper limits of mixed temperature of return networks, respectively.

Constrains (A1) and (A4)-(A18) are abbreviated as:

$$\boldsymbol{F}_{\mathrm{C}(a)}\boldsymbol{h}_{\mathrm{C}}+\boldsymbol{F}_{\mathrm{H}(a)}\boldsymbol{h}_{\mathrm{H}(a)}+\boldsymbol{D}_{\mathrm{H}(a)}\boldsymbol{x}_{\mathrm{H}(a)}=\boldsymbol{f}_{\mathrm{H}(a)} \tag{A21}$$

Constrains (A19) and (A20) are collapsed into:

$$\underline{\boldsymbol{x}}_{\mathrm{H}(a)}\le\boldsymbol{x}_{\mathrm{H}(a)}\le\bar{\boldsymbol{x}}_{\mathrm{H}(a)} \tag{A22}$$

where $\underline{\boldsymbol{x}}_{\mathrm{H}(a)}$ and $\bar{\boldsymbol{x}}_{\mathrm{H}(a)}$ are the lower and upper limits of the internal variable vector of the a^{th} DHN, respectively.

Constraints (A3), (A19), and (A20) are written as:

$$\boldsymbol{G}_{\mathrm{C}(a)}^{\mathrm{FC}}\boldsymbol{h}_{\mathrm{C}}+\boldsymbol{G}_{\mathrm{H}(a)}^{\mathrm{FC}}\boldsymbol{h}_{\mathrm{H}(a)}\le\boldsymbol{g}_{(a)}^{\mathrm{FC}} \tag{A23}$$

$$\boldsymbol{G}_{\mathrm{C}(a)}^{\mathrm{FC}}=\begin{bmatrix}-\boldsymbol{D}_{\mathrm{H}(a)}^{-1}\boldsymbol{F}_{\mathrm{C}(a)}\\ \boldsymbol{D}_{\mathrm{H}(a)}^{-1}\boldsymbol{F}_{\mathrm{C}(a)}\\ \boldsymbol{0}\\ \boldsymbol{0}\end{bmatrix} \tag{A24}$$

$$\boldsymbol{G}_{\mathrm{H}(a)}^{\mathrm{FC}}=\begin{bmatrix}-\boldsymbol{D}_{\mathrm{H}(a)}^{-1}\boldsymbol{F}_{\mathrm{H}(a)}\\ \boldsymbol{D}_{\mathrm{H}(a)}^{-1}\boldsymbol{F}_{\mathrm{H}(a)}\\ \boldsymbol{I}\\ -\boldsymbol{I}\end{bmatrix} \tag{A25}$$

$$\boldsymbol{g}_{(a)}^{\mathrm{FC}}=\begin{bmatrix}\bar{\boldsymbol{x}}_{\mathrm{H}(a)}-\boldsymbol{D}_{\mathrm{H}(a)}^{-1}\boldsymbol{f}_{\mathrm{H}(a)}\\ \boldsymbol{D}_{\mathrm{H}(a)}^{-1}\boldsymbol{f}_{\mathrm{H}(a)}-\underline{\boldsymbol{x}}_{\mathrm{H}(a)}\\ \bar{\boldsymbol{h}}_{\mathrm{H}(a)}\\ -\underline{\boldsymbol{h}}_{\mathrm{H}(a)}\end{bmatrix} \tag{A26}$$

Detailed descriptions of $\boldsymbol{F}_{\mathrm{C}(a)}$, $\boldsymbol{F}_{\mathrm{H}(a)}$, $\boldsymbol{D}_{\mathrm{H}(a)}$, $\boldsymbol{f}_{\mathrm{H}(a)}$, $\boldsymbol{G}_{\mathrm{C}(a)}^{\mathrm{FC}}$, $\boldsymbol{G}_{\mathrm{H}(a)}^{\mathrm{FC}}$, and $\boldsymbol{g}_{\mathrm{C}(a)}^{\mathrm{FC}}$ are available in [30], [31].

B. Economic Dispatch Model for EPN

According to the DC power flow model, an EPN economic dispatch model is established, including CHP units, thermal generating units, and wind farms. The objective function of the model is to minimize the total cost of IEHS.

1) Objective Function

$$\min\sum_{t\in\mathcal{T}}\left(\sum_{g\in\mathcal{G}^{\mathrm{TU}}}C_g^{\mathrm{TU}}+\sum_{g\in\mathcal{G}^{\mathrm{CHP}}}C_g^{\mathrm{CHP}}+\sum_{g\in\mathcal{G}^{\mathrm{wind}}}C_g^{\mathrm{wind}}\right) \tag{A27}$$

where $\mathcal{G}^{\mathrm{TU}}$, $\mathcal{G}^{\mathrm{CHP}}$, and $\mathcal{G}^{\mathrm{wind}}$ are the sets of thermal generating units, CHP units, and wind farms, respectively; C_g^{TU}, C_g^{CHP}, and C_g^{wind} are the operating costs of thermal generating units, CHP units, and wind farms, respectively; and $\mathcal{T}$ is the set of dispatch horizons.

1) CHP units

The operating cost of CHP unit g is:

$$\begin{aligned}C_g^{\mathrm{CHP}}\left(p_{g,t},h_{g,t}\right)=&c_g^{\mathrm{E},2}p_{g,t}^2+c_g^{\mathrm{H},2}h_{g,t}^2+c_g^{\mathrm{E,H}}p_{g,t}h_{g,t}+\\ &c_g^{\mathrm{E},1}p_{g,t}+c_g^{\mathrm{H},1}h_{g,t}+c_g^0\quad\forall g\in\mathcal{G}^{\mathrm{CHP}},\forall t\in\mathcal{T}\end{aligned} \tag{A28}$$

where $c_g^{\mathrm{E},2}$, $c_g^{\mathrm{H},2}$, $c_g^{\mathrm{E,H}}$, $c_g^{\mathrm{E},1}$, $c_g^{\mathrm{H},1}$, and c_g^0 are the operating cost coefficients; and $p_{g,t}$, and $h_{g,t}$ are the power and heat outputs of unit g during period t, respectively.

$$\begin{cases}p_{g,t}=\sum_{m=1}^{NK_g}\alpha_{g,t}^m P_g^m\\ h_{g,t}=\sum_{m=1}^{NK_g}\alpha_{g,t}^m H_g^m\end{cases}\quad\forall g\in\mathcal{G}^{\mathrm{CHP}},\forall t\in\mathcal{T} \tag{A29}$$

$$\begin{cases}\sum_{m=1}^{NK_g}\alpha_{g,t}^m=1\\ 0\le\alpha_{g,t}^m\le1\end{cases}\quad\forall g\in\mathcal{G}^{\mathrm{CHP}},m\in\left\{1,2,\ldots,NK_g\right\},t\in\mathcal{T} \tag{A30}$$

where $\alpha_{g,t}^m$ is the m^{th} extreme point of CHP unit g during period t; P_g^m and H_g^m are the power and heat generations at the m^{th} extreme point of CHP unit g, respectively; and NK_g is the number of extreme point of CHP unit g.

2) Thermal generating units

The operating cost of thermal generating units g is:

$$C_g^{\mathrm{TU}}\left(p_{g,t}\right)=c_g^{\mathrm{TU},2}p_{g,t}^2+c_g^{\mathrm{TU},1}p_{g,t}+c_g^{\mathrm{TU},0}\quad\forall g\in\mathcal{G}^{\mathrm{TU}},\forall t\in\mathcal{T} \tag{A31}$$

where $c_g^{\mathrm{TU},2}$, $c_g^{\mathrm{TU},1}$, and $c_g^{\mathrm{TU},0}$ are the operating cost coefficients.

3) Wind farms

The penalty cost for wind curtailments is:

$$C_g^{\mathrm{wind}}\left(p_{g,t}^{\mathrm{w}}\right)=\sigma_g\left(\bar{P}_{g,t}^{\mathrm{w}}-p_{g,t}^{\mathrm{w}}\right)^2\quad\forall g\in\mathcal{G}^{\mathrm{wind}},\forall t\in\mathcal{T} \tag{A32}$$

where σ_g is the penalty factor in wind farm g; $\bar{P}_{g,t}^{\mathrm{w}}$ is the forecast output of wind farm g during period t; and $p_{g,t}^{\mathrm{w}}$ is the pow-

er output of wind farm g during period t.

2) Constraints

1) Active power balance

$$\sum_{g\in\mathcal{G}^{\mathrm{TU}}\bigcup\mathcal{G}^{\mathrm{CHP}}} p_{g,t}+\sum_{g\in\mathcal{G}^{\mathrm{wind}}} p_{g,t}^{\mathrm{w}}=\sum_{i\in\mathcal{G}^{\mathrm{bus}}} D_{i,t}+\sum(\theta_{i,t}-\theta_{j,t})/X_{i,j}\quad t\in\mathcal{T} \tag{A33}$$

where $\mathcal{G}^{\mathrm{bus}}$ is the set of buses; $D_{i,t}$ is the power load of bus i during period t; $\theta_{i,t}$ is the phase angle of bus i during period t; and $X_{i,j}$ is the reactance between bus i and bus j.

2) Spinning reserve constraints

$$p_{g,t}+ru_{g,t}\le\bar{P}_g\quad\forall t\in\mathcal{T},g\in\mathcal{G}^{\mathrm{TU}} \tag{A34}$$

$$p_{g,t}-rd_{g,t}\ge\underline{P}_g\quad\forall t\in\mathcal{T},g\in\mathcal{G}^{\mathrm{TU}} \tag{A35}$$

$$\begin{cases}\sum_{g\in\mathcal{G}^{\mathrm{TU}}} ru_{g,t}\ge SR^{\mathrm{up}}\\ \sum_{g\in\mathcal{G}^{\mathrm{TU}}} rd_{g,t}\ge SR^{\mathrm{down}}\end{cases}\quad\forall t\in\mathcal{T} \tag{A36}$$

$$\begin{cases}0\le ru_{g,t}\le RAMP_g^{\mathrm{up}}\cdot\Delta t\\ 0\le rd_{g,t}\le RAMP_g^{\mathrm{down}}\cdot\Delta t\end{cases}\quad\forall t\in\mathcal{T},g\in\mathcal{G}^{\mathrm{TU}} \tag{A37}$$

where $ru_{g,t}$ and $rd_{g,t}$ are the upward and downward spinning reserve capacities of generation unit g during period t, respectively; $\bar{P}_g$ and $\underline{P}_g$ are the upper and lower limits of generation of CHP units and thermal generating units, respectively; SR^{up} and SR^{down} are the upward and downward spinning reserve demands during period t, respectively; and $RAMP_g^{\mathrm{up}}$ and $RAMP_g^{\mathrm{down}}$ are the upward and downward ramp rates of generation unit g, respectively.

3) Ramping limits

$$-RAMP_g^{\mathrm{down}}\cdot\Delta t\le p_{g,t}-p_{g,t-1}\le RAMP_g^{\mathrm{up}}\cdot\Delta t\quad\forall g\in\mathcal{G}^{\mathrm{TU}}\bigcup\mathcal{G}^{\mathrm{CHP}},t\in\mathcal{T} \tag{A38}$$

4) Power network constraints

$$-P_{i,j}\le(\theta_{i,t}-\theta_{j,t})/X_{i,j}\le P_{i,j}\quad\forall t\in\mathcal{T} \tag{A39}$$

$$\theta_{\mathrm{ref},t}=0 \tag{A40}$$

where $\theta_{\mathrm{ref},t}$ is the phase angle reference bus during period t.

5) Output limits

CHP units and thermal generating units are subject to operating limits.

$$\underline{P}_g\le p_{g,t}\le\bar{P}_g\quad\forall g\in\mathcal{G}^{\mathrm{CHP}},\forall t\in T \tag{A41}$$

6) Generation capacity

Generation should not exceed its capacity.

$$0\le p_{g,t}^{\mathrm{w}}\le\bar{P}_g^{\mathrm{w}}\quad\forall g\in\mathcal{G}^{\mathrm{wind}},\forall t\in T \tag{A42}$$

REFERENCES

[1] B. C. Ummels, M. Gibescu, E. Pelgrum *et al*., "Impacts of wind power on thermal generation unit commitment and dispatch," *IEEE Transactions on Energy Conversion*, vol. 22, no. 1, pp. 44-51, Mar. 2007.

[2] CREIA, CWEA, GWEC. (2022, Jan.). China wind power review and outlook 2014. [Online]. Available: https://www.gwec.net/wp-content/uploads/2012/06/2014%E9%A3%8E% E7%94%B5%E6%8A% A5%E5%91%8A2%E8%8B%B1%E6%96%87-20150317.pdf

[3] X. Chen, C. Kang, M. O'Malley *et al*., "Increasing the flexibility of combined heat and power for wind power integration in china: modeling and implications," *IEEE Transactions on Power Systems*, vol. 30, no. 4, pp. 1848-1857, Jul. 2015.

[4] G. Papaefthymiou, B. Hasche, and C. Nabe, "Potential of heat pumps for demand side management and wind power integration in the german electricity market," *IEEE Transactions on Sustainable Energy*, vol. 3, no. 4, pp. 636-642, Oct. 2012.

[5] B. Rolfsman, "Combined heat-and-power plants and district heating in a deregulated electricity market," *Applied Energy*, vol. 78, no. 1, pp. 37-52, May 2004.

[6] Z. Li, W. Wu, M. Shahidehpour *et al*., "Combined heat and power dispatch considering pipeline energy storage of district heating network," *IEEE Transactions on Sustainable Energy*, vol. 7, no. 1, pp. 12-22, Jan. 2016.

[7] X. Liu, J. Wu, N. Jenkins *et al*., "Combined analysis of electricity and heat networks," *Applied Energy*, vol. 162, pp. 1238-1250, Jan. 2016.

[8] W. Wang, S. Huang, G. Zhang *et al*., "Optimal operation of an integrated electricity-heat energy system considering flexible resources dispatch for renewable integration," *Journal of Modern Power Systems and Clean Energy*, vol. 9, no. 4, pp. 699-710, Jul. 2021.

[9] S. Lu, W. Gu, S. Zhou *et al*., "High-resolution modeling and decentralized dispatch of heat and electricity integrated energy system," *IEEE Transactions on Sustainable Energy*, vol. 11, no. 3, pp. 1451-1463, Jul. 2020.

[10] Y. Chen, Q. Guo, and H. Sun, "Decentralized unit commitment in integrated heat and electricity systems using SDM-GS-ALM," *IEEE Transactions on Power Systems*, vol. 34, no. 3, pp. 2322-2333, May 2019.

[11] H. N. Tran, T. Narikiyo, M. Kawanishi *et al*., "Whole-day optimal operation of multiple combined heat and power systems by alternating direction method of multipliers and consensus theory," *Energy Conversion and Management*, vol. 174, pp. 475-488, Oct. 2018.

[12] T. Zhang, Z. Li, Q. Wu *et al*., "Decentralized state estimation of combined heat and power systems using the asynchronous alternating direction method of multipliers," *Applied Energy*, vol. 248, pp. 600-613, Aug. 2019.

[13] H. R. Abdolmohammadi and A. Kazemi, "A Benders decomposition approach for a combined heat and power economic dispatch," *Energy Conversion and Management*, vol. 71, pp. 21-31, Jul. 2013.

[14] H. R. Sadeghian and M. M. Ardehali, "A novel approach for optimal economic dispatch scheduling of integrated combined heat and power systems for maximum economic profit and minimum environmental emissions based on Benders decomposition," *Energy*, vol. 102, pp. 10-23, May 2016.

[15] C. Lin, W. Wu, B. Zhang *et al*., "Decentralized solution for combined heat and power dispatch through benders decomposition," *IEEE Transactions on Sustainable Energy*, vol. 8, no. 4, pp. 1361-1372, Oct. 2017.

[16] J. Huang, Z. Li, and Q. Wu, "Coordinated dispatch of electric power and district heating networks: a decentralized solution using optimality condition decomposition," *Applied Energy*, vol. 206, pp. 1508-1522, Nov. 2017.

[17] Z. Yi, Y. Xu, J. Hu *et al*., "Distributed, neurodynamic-based approach for economic dispatch in an integrated energy system," *IEEE Transactions on Industrial Informatics*, vol. 16, no. 4, pp. 2245-2257, Apr. 2020.

[18] N. Liu, J. Wang, and L. Wang, "Hybrid energy sharing for multiple microgrids in an integrated heat-electricity energy system," *IEEE Transactions on Sustainable Energy*, vol. 10, no. 3, pp. 1139-1151, Jul. 2019.

[19] L. Deng, Z. Li, H. Sun *et al*., "Generalized locational marginal pricing in a heat-and-electricity-integrated market," *IEEE Transactions on Smart Grid*, vol. 10, no. 6, pp. 6414-6425, Nov. 2019.

[20] W. Zheng, J. Zhu, and Q. Luo, "Distributed dispatch of integrated electricity-heat systems with variable mass flow," *IEEE Transactions on Smart Grid*. doi: 10.1109/TSG.2022.3210014

[21] Y. Chen, W. Wei, F. Liu *et al*., "Energy trading and market equilibrium in integrated heat-power distribution systems," *IEEE Transactions on Smart Grid*, vol. 10, no. 4, pp. 4080-4094, Jul. 2019.

[22] J. Wei, Y. Zhang, J Wang *et al*., "Decentralized demand management based on alternating direction method of multipliers algorithm for industrial park with CHP units and thermal storage," *Journal of Modern Power Systems and Clean Energy*, vol. 10, no. 1, pp. 120-130, Jan. 2022.

[23] J. Yang, A. Botterud, N. Zhang *et al*., "A cost-sharing approach for decentralized electricity-heat operation with renewables," *IEEE Transactions on Sustainable Energy*, vol. 11, no. 3, pp. 1838-1847, Jul. 2020.

[24] B. Chen, W. Wu, and H. Sun, "Coordinated heat and power dispatch considering mutual benefit and mutual trust: a multi-party perspective," *IEEE Transactions on Sustainable Energy*, vol. 13, no. 1, pp. 251-264, Jan. 2022.

[25] A. E. Roth, *Introduction to the Shapley Value.* New York: Cambridge University Press, 1988.
[26] Y. Guo, L. Tong, W. Wu *et al*., "Coordinated multi-area economic dispatch via critical region projection," *IEEE Transactions on Power Systems*, vol. 32, no. 5, pp. 3736-3746, Sept. 2017.
[27] Gurobi Optimization. (2022, Feb.). Gurobi. [Online]. Available: http://www.gurobi.com/
[28] H. Zhu. (2022, Mar.). Test data of two integrated electricity and heat systems. [Online]. Available: https://doi.org/10.6084/m9.figshare.19432040
[29] Y. Dai, L. Chen, Y. Min *et al*., "Dispatch model of combined heat and power plant considering heat transfer process," *IEEE Transactions on Sustainable Energy*, vol. 8, no. 3, pp. 1225-1236, Jul. 2017.
[30] W. Zheng and D. J. Hill, "Distributed real-time dispatch of integrated electricity and heat systems with guaranteed feasibility," *IEEE Transactions on Industrial Informatics*, vol. 18, no. 2, pp. 1175-1185, Feb. 2022.
[31] W. Zheng, Y. Hou, and Z. Li, "A dynamic equivalent model for district heating networks: formulation, existence and application in distributed electricity-heat operation," *IEEE Transactions on Smart Grid*, vol. 12, no. 3, pp. 2685-2695, May 2021.

Jizhong Zhu received the B.S., M.S., and Ph.D. degrees in electrical engineering from Chongqing University, Chongqing, China, in 1985, 1987, and 1990, respectively. He is currently working as a Professor in South China University of Technology, Guangzhou, China. His research interests include power system operation and control as well as renewable energy application.

Haohao Zhu received the B.S. degree in electrical engineering from Nanchang University, Nanchang, China, in 2020. He is currently pursuing the M.S. degree in electrical engineering in South China University of Technology, Guangzhou, China. His research interests include distributed optimal dispatch of integrated electricity-heat systems.

Weiye Zheng received the B.S. and Ph.D. degrees in electrical engineering from Tsinghua University, Beijing, China, in 2013 and 2018, respectively. He is currently working as an Associate Professor in South China University of Technology, Guangzhou, China. His research interests include analysis, operation and market in integrated energy systems.

Shenglin Li received the B.S. and M.S. degrees in electrical engineering from Shanghai University of Electric Power, Shanghai, China, in 2016 and 2019, respectively. He is currently pursuing the Ph.D. degree in electrical engineering in South China University of Technology, Guangzhou, China. His research interests include energy management of renewable energy microgrids and active distribution networks.

Junwei Fan received the B.S. degree in electrical engineering from China University of Mining and Technology, Xuzhou, China, in 2020. He is currently working toward the M.S. degree in electrical engineering in South China University of Technology, Guangzhou, China. His research interests include electricity market and energy blockchain.